Sensors & Actuators: B. Chemical 334 (2021) 129608

Contents lists available at ScienceDirect

Sensors and Actuators: B. Chemical

journal homepage: www.elsevier.com/locate/snb

A duple nanozyme stimulating tandem catalysis assisted multiple signal inhibition strategy for photoelectrochemical bioanalysis

Yanrong Qian [a], Yu Du [a], Jinhui Feng [a], Rui Xu [a], Xiang Ren [a], Dawei Fan [a], Qin Wei [a,*], Huangxian Ju [a,b,*]

[a] Collaborative Innovation Center for Green Chemical Manufacturing and Accurate Detection, University of Jinan, Jinan, 250022, Shandong, China
[b] State Key Laboratory of Analytical Chemistry for Life Science, Department of Chemistry, Nanjing University, Nanjing, 210023, China

ARTICLE INFO

Keywords:
Photoelectrochemical
Nanozyme
Biocatalytic precipitation
Bismuth oxysulfide
Signal inhibition

ABSTRACT

A sandwich-type photoelectrochemical (PEC) immunosensor was developed for cytokeratin 19 fragment 21−1 (CYFRA21−1) ultrasensitive detection relying on a multiple signal inhibition strategy. In this work, $Bi_{10}O_6S_9$ nanosheet arrays (BiOS) sensitized strontium titanate nanocubes ($SrTiO_3$ NCs) was used as photoactive matrix. $Bi_{10}O_6S_9$ with the large specific surface area and narrow band gap could improve the utilization of light to provide strong initial PEC signal. Besides, bovine serum albumin stabilized gold nanoparticles (BSA@Au NPs) anchored on Cu_7S_4 polyhedron composite (BSA-Au@Cu_7S_4 polyhedron) was utilized as an effective PEC signal regulator. As a duple nanozyme with the glucose oxidase (GOx)-like activity and the peroxidase-like activity, BSA@Au NPs induced intriguing tandem biocatalytic precipitation (BCP). On the one hand, the BCP could produce precipitations which obstructed the electron transfer between the photoelectrode and electron donor, leading a decrease of PEC signal; On the other hand, the competitive light absorption between BSA-Au@Cu_7S_4 polyhedron and photoactive matrix caused a further reduction of PEC signal. Generally, the PEC signal was quenched sharply taking advantage of multiple signal inhibition strategy including tandem BCP strategy, competitive absorption of light and steric hindrance, which improved the detection sensitivity of PEC immunosensor. The suggested PEC immunosensor displayed a good linearity in the range of 0.1 pg/mL - 50 ng/mL for CYFRA21−1 detection with a low detection limit of 1.12 fg/mL (S/N = 3). The skillful strategy has infinite potential in biological samples analysis.

1. Introduction

Biosensor, known as a vigorously rising analytical method which transforms specific biorecognition events into readable signal has drawn growing attention for decades in bioanalytical areas including nucleic acids detection, immunoassays, enzyme detection and so on [1–3]. Thereinto, photoelectrochemical (PEC) biosensor is a primary detection method. Generally, quantitative analysis with PEC immunosensor is based on photoelectron transfer of electrode/electrolyte interface and subsequent electrical signal changes after specific recognition [4,5]. PEC immunosensor converts the light source excitation signal into a displayable electrical signal and it has high sensitivity and low background due to inconsistency of excitation source and detection signal.

Photoactive matrix is a component for PEC immunosensor and its brilliant performance is important for producing satisfactory photocurrent signal. Most recently, strontium titanate ($SrTiO_3$), a significant multimetallic oxide perovskite, has been widely applied in solar cells, photocatalytic water splitting and so on [6–8]. What is more, with similar band gap structure to titanium dioxide, $SrTiO_3$ also owns prospective application potential in PEC bioanalysis [9]. However, the absorption of $SrTiO_3$ is limited in the ultraviolet (UV) light region where irradiation source causes biomolecule damage owing to the wide band gap [10]. To further increase the harvesting of visible light, compounding $SrTiO_3$ with narrow band gap semiconductor materials is a valid method [11]. Given the brilliant photoactive, electrical and eco-friendly properties, various Bi-based materials such as bismuth salt, bismuth oxyhalides and bismuth oxysulfide have caused wide public concern [12–15]. As a promising layered material, bismuth oxysulfide stands out in the light absorption among of Bi-based semiconductors due to narrow band gap. Therefore, $Bi_{10}O_6S_9$ (BiOS) nanosheet arrays were

* Corresponding authors at: Collaborative Innovation Center for Green Chemical Manufacturing and Accurate Detection, University of Jinan, Jinan, 250022, Shandong, China.
E-mail addresses: sdjndxwq@163.com (Q. Wei), hxju@nju.edu.cn (H. Ju).

https://doi.org/10.1016/j.snb.2021.129608
Received 17 December 2020; Received in revised form 28 January 2021; Accepted 31 January 2021
Available online 9 February 2021

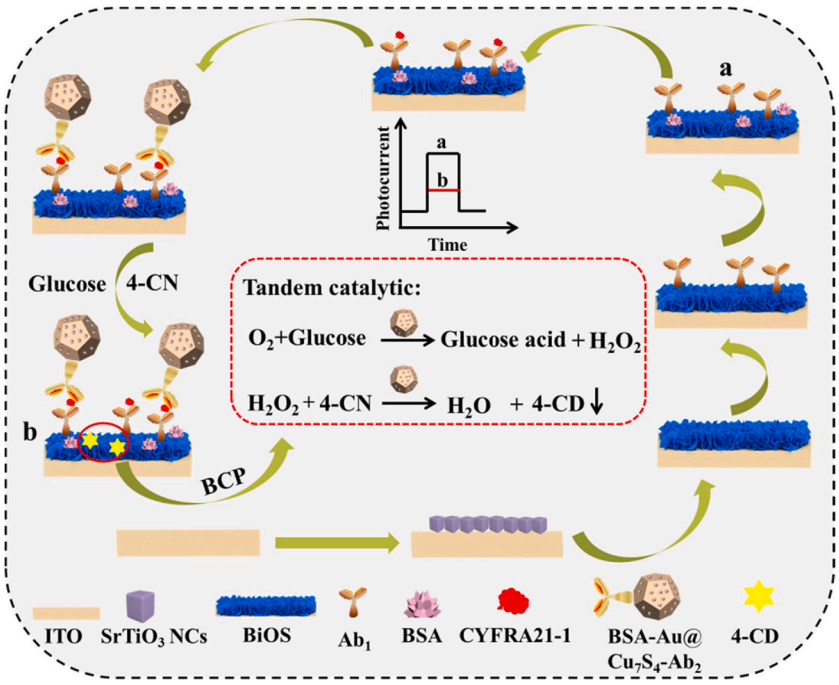

Scheme 1. Assembly process of the proposed PEC sensing platform for detecting CYFRA21-1.

utilized to broaden the light absorption range of strontium titanate nanocubes ($SrTiO_3$ NCs). And it's worth mentioning that the randomly oriented nanosheet array thin films of BiOS possessed low recombination losses and increased PEC response. Nevertheless, constructing label-free PEC immunosensor directly based on the BiOS nanosheet arrays sensitized $SrTiO_3$ nanocubes ($SrTiO_3$/BiOS) may lead to insufficient sensitivity when detecting analytes [16]. Consequently, signal regulation strategy plays a vital role in the construction process of ultrasensitive PEC biosensors.

Among a variety of strategies, biocatalytic precipitation (BCP) is a convenient and effective method, in which the insoluble sediment formation making use of the catalysis of enzymes affected PEC response [17,18]. It is noteworthy apparently that the choice of enzyme plays a hard-core role in BCP strategy. Previously, natural enzymes are preferred in a large number of PEC immunoassays. For example, alkaline phosphate (ALP) catalyzes 5-bromo-4-chloro-3-indoyl phosphate (BCIP) to yield precipitation and resulting in the suppression of the photocurrent responses [19]. However, natural enzymes are impressible to external environment and liable to denaturation and inactivation. To overcome this bottleneck, a lot of mimic enzymes are developed with the advancements in nanomaterials. As a promising substitute for natural enzymes, nanoenzymes have advantages of excellent stability and unique enzyme-like capabilities, which broaden new path for biodetection [20–22]. Noble-metal nanoparticles display good biocompatibility and catalytic activity [23]. As representative mimic enzyme, it was reported that gold nanoparticals stabilized by bovine serum albumin (BSA@Au NPs) have dual enzyme-like activities including glucose oxidase (GOx)-like activity and peroxidase-like activity [24]. It was indicated that BSA@Au NPs can perform tandem catalysis to catalyze the production of hydrogen peroxide (H_2O_2) from glucose and the further reaction between 4-chloro-1-naphthol (4-CN) and H_2O_2 was conveniently catalyzed to form insoluble and nonconductive benzo-4-chlorohexadienone (4-CD). Besides, copper sulfide nanocrystallites (Cu_xS_y) have aroused increasing attention in PEC area due to the excellent light absorption and the peroxidase-mimicking activities, which make them become outstanding signal regulators in PEC immunoassay [25–27]. In order to load more BSA@Au NPs and biomolecules, polyhedron Cu_7S_4 was prepared. Its peroxidase-mimicking catalytic property and large specific surface area were beneficial to the occurrence of tandem catalysis in BCP strategy [28]. Based on the above analysis, BSA@Au NPs anchored on the Cu_7S_4 polyhedron (BSA-Au@Cu_7S_4 polyhedron) was chosen as signal quencher in the BCP strategy which altered the interfacial electron-transfer property and reduced the PEC response produced by $SrTiO_3$/BiOS.

Over here, a sandwich-type PEC immunosensor was constructed for target analyte basing on the BiOS nanosheet arrays sensitized $SrTiO_3$ nanocubes ($SrTiO_3$/BiOS) as photoactive substance providing initial photocurrent and BSA-Au@Cu_7S_4 polyhedron as a signal regulator to realize multiple signal inhibition strategy. BiOS nanosheet arrays sensitized $SrTiO_3$ NCs prompted the electron transfer with the assistance of electron donor and improved sharply PEC response in the visible light region. In view of Cu_7S_4 as a solar absorber with strong vis-NIR absorption [29,30] and dual enzyme-like activities of BSA@Au NPs, BSA-Au@Cu_7S_4 polyhedron took advantage of BCP strategy, competitive absorption of light and steric hindrance to reduce photocurrent. In this work, cytokeratin 19 fragment 21−1 (CYFRA21−1), as a target example, is a reliable biomarker for squamous cell carcinomas. This strategy will broaden new horizons for designing facile, biocompatible, and eco-friendly PEC biosensors.

2. Experimental section

2.1. Reagents and apparatus

The reagents and apparatus utilized in this work could be found in the Supporting Information (SI) file.

2.2. Preparation of BiOS nanosheet arrays

Previous to use, indium tin oxide (ITO) electrodes were disposed using acetone, ethanol and ultrapure water severally, and then dried with nitrogen. The $SrTiO_3$ nanocubes were prepared via the controllable hydrolysis of tetrabutyl titanate as shown in SI [31]. The BiOS nanosheet arrays were synthesized with the method of chemical bath deposition [32]. At first, 0.50 g $Bi(NO_3)_3{\cdot}5H_2O$ was dissolved in 5.60 g triethanolamine to form a transparent solution. Then, 0.79 g thiourea and 0.50

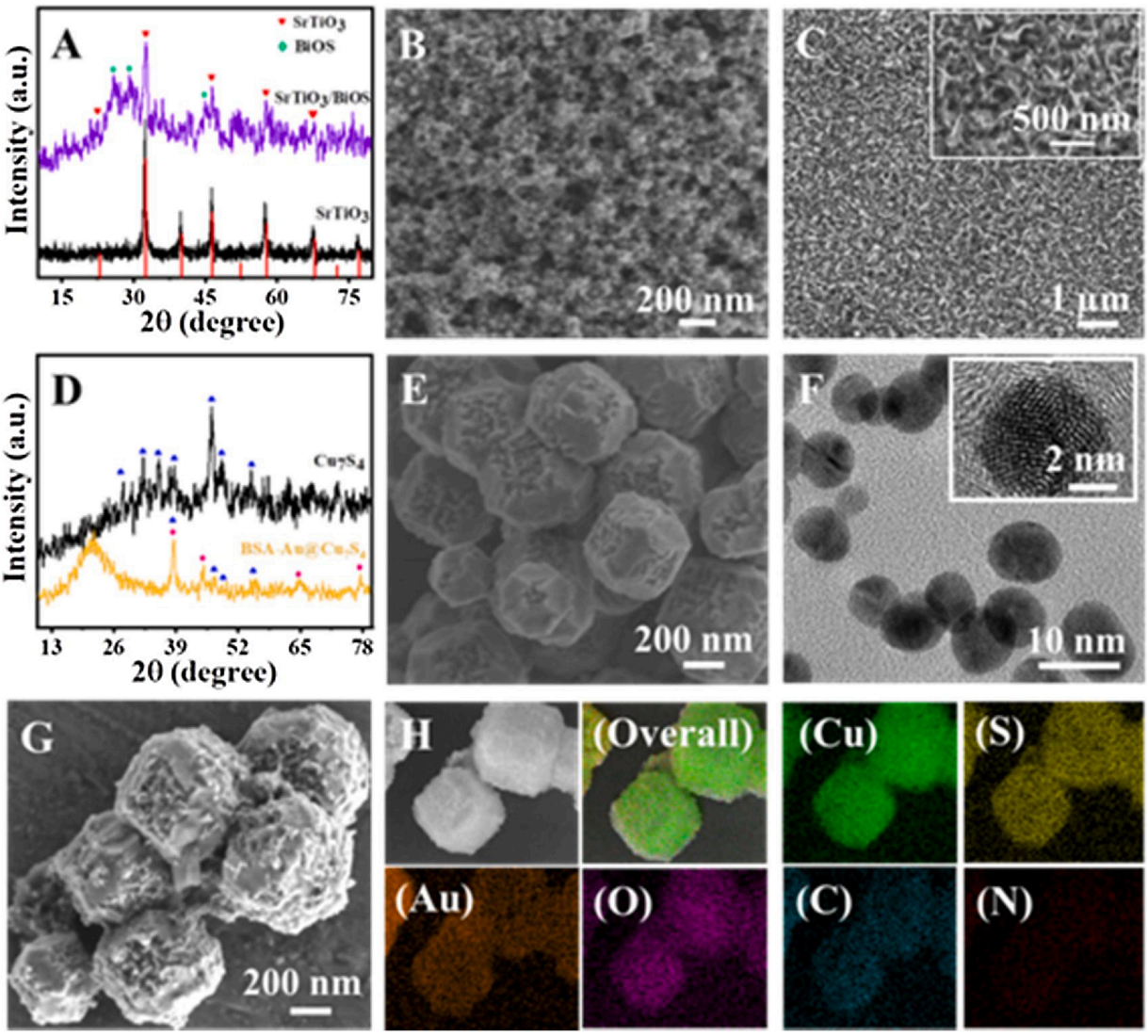

Fig. 1. (A) XRD pattern of $SrTiO_3$ NCs and BiOS nanosheet arrays; (B) and (C) SEM images of $SrTiO_3$ NCs and BiOS nanosheet arrays; (D) XRD pattern of Cu_7S_4 polyhedron and BSA-Au@Cu_7S_4 polyhedron; (E) SEM image of Cu_7S_4 polyhedron; (F) TEM and HRTEM image (inset) of BSA@Au NPs; (G) SEM image and (H) Elemental mapping of BSA-Au@Cu_7S_4 polyhedron.

mL NH_4OH (25–28 % wt) were added to the mentioned mixture and diluted into a final volume of 50 mL. Finally, an ITO electrode was immersed into 1.50 mL above solution maintaining at 100 ℃ for 50 min. The acquired product was washed several times by ultrapure water.

2.3. Preparation of BSA@Au NPs

Cu_7S_4 polyhedron was prepared according the previous literature displayed in the SI [26]. BSA@Au NPs was prepared utilizing reduction of chloroauric acid by sodium borohydride with BSA as stabilizer [24]. Firstly, 0.0034 g BSA was dissolved into 4 mL deionized water. Then, 1 mL of chloroauric acid (24.3×10^{-3} mol/L) was added into above BSA solution. After stirring for 1 h, 100 μL of $NaBH_4$ (1 mg/mL) was added into the above reaction system and magnetic stirred for 0.5 h. The acquired BSA@Au NPs were stored at 4 ℃.

2.4. Assembly process of the proposed PEC immunosensor

The fabrication of suggested PEC immunosensor was illustrated in Scheme 1. At first, 10 μL of $SrTiO_3$ NCs (6 mg/mL) suspension was dipped to the ITO electrode. After dried at the room temperature, ITO/$SrTiO_3$ electrode was calcinated at 200 ℃ for 1 h in a muffle furnace. Followed by cooled to the room temperature, the BiOS nanosheet arrays grow on the ITO/$SrTiO_3$ electrode in the light of the above steps in the section 2.1 to gain the ITO/$SrTiO_3$/BiOS electrode. Then the ITO/$SrTiO_3$/BiOS electrode was modified with 4 μL of thioglycolic acid (TGA) (3 mmol/L). For activing the −COOH group, 3 μL of EDC/NHS was covered on the mentioned electrode. After each of the above steps, electrode was rinsed with deionized water. Subsequently, 6 μL of Ab_1 (10 μg/mL) was drop onto the ITO/$SrTiO_3$/BiOS electrode and then 3 μL of BSA (1% wt) was added onto the above electrode to block non-specific binding sites. Afterwards, different concentrations of CYFRA21−1 were applied for specific recognition with Ab_1. After that, 6 μL of BSA-Au@Cu_7S_4-Ab_2 (2.5 mg/mL) was incubated on the above electrode. Each of the above steps involving biomolecules was carried out at 4 ℃ for 60 min and thoroughly washed with PBS (pH 7.4). Finally, the aforesaid electrode was immersed into 5 mM glucose and 5 mM 4-chloro-1-naphthol (4-CN) for 30 min at room temperature, respectively.

3. Results and discussion

3.1. Characterization of prepared materials

X-ray powder diffraction spectra (XRD), scanning electron

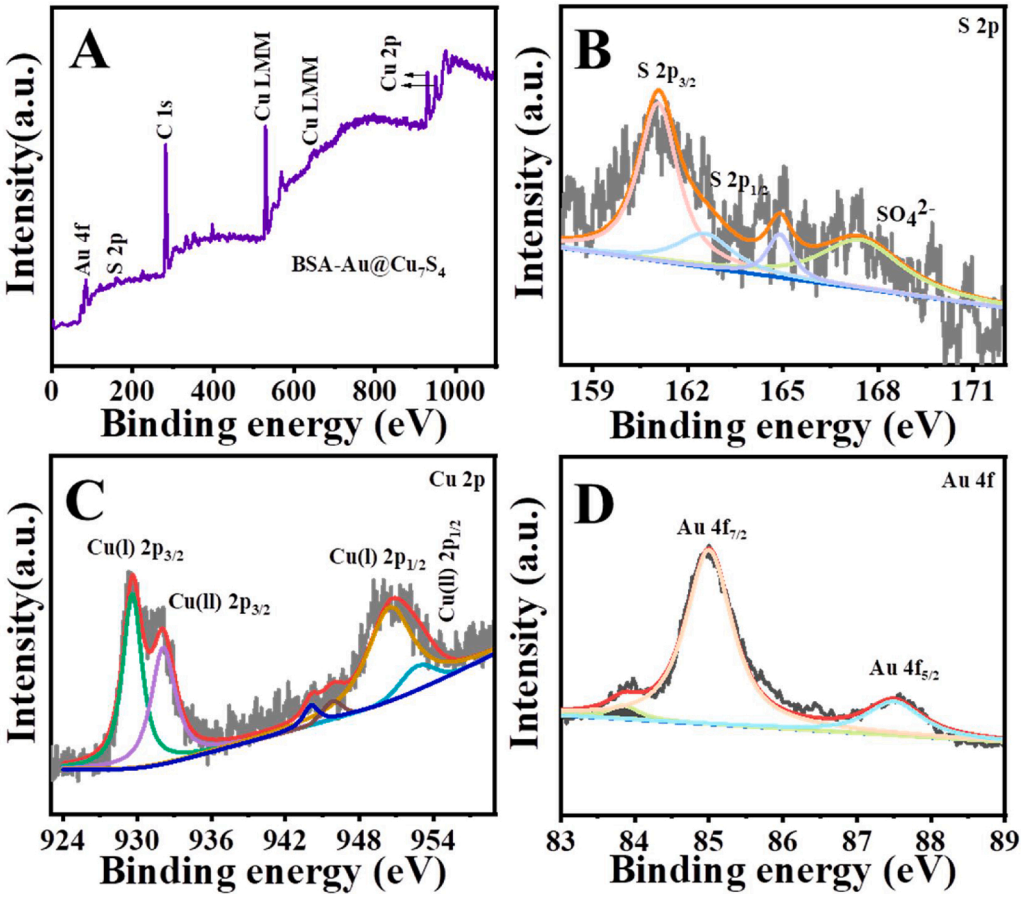

Fig. 2. (A) XPS survey pattern of BSA-Au@Cu_7S_4 polyhedron and the high-resolution XPS spectra of (B) S 2p, (C) Cu 2p, (D) Au 4f.

microscopy (SEM), X-ray photoelectron spectra (XPS) and so on were utilized to reveal the structural and compositional information of the as-fabricated materials. Primarily, the crystal structures of $SrTiO_3$ NCs and BiOS nanosheet arrays were distinguished by XRD as shown in Fig. 1A. All the observed diffraction peaks for synthesized pure $SrTiO_3$ NCs centered at 22.78°, 32.42°, 46.48°, 57.79° and 67.80° were corresponding to (100), (110), (200), (211) and (220) diffraction planes of tausonite $SrTiO_3$ (JCPDS No.35−0734). For the ITO/$SrTiO_3$/BiOS electrode, auxiliary weak diffraction peaks appeared at 25.11°, 28.42° and 44.38° could be assigned to BiOS nanosheet arrays in literature reports [33]. Simultaneously, Fig. 1B and Fig S1A showed the morphology of $SrTiO_3$ nanocubes, increasing the roughness of the ITO electrode for the growth of BiOS nanosheet arrays. In Fig. 1C and its inset, BiOS showed a highly-developed nanoarray structure that grew densely in a radial manner on $SrTiO_3$ nanocubes, providing large specific surface area for light-harvesting and biomolecule-loading [34]. In Fig S1 B and C, energy-dispersive spectroscopy (EDS) and element mapping illustrated that Sr, Ti, O, Bi and S elements were existed and uniformly dispersed on ITO/$SrTiO_3$/BiOS electrode.

The XRD pattern of Cu_7S_4 polyhedron was displayed in the Fig. 1D. The peaks appeared at 27.88°, 32.30°, 35.34°, 37.77°, 46.46°, 48.34°, and 54.64° were in accordance with (022), (004), (031), (302), (040), (323) and (422) in crystallographic planes (JCPDS No. 33-0489). After BSA@Au NPs anchored on Cu_7S_4 polyhedron, the new peaks arose at 38.18°, 44.39°, 64.58° and 77.55° were vested in BSA@Au NPs (JCPDS No. 04-0784). However, the peaks of Cu_7S_4 polyhedron were weakened due to the existence of BSA on the surface. In Fig. 1E, the Cu_7S_4 polyhedron possessed 18 facets with an average size of about 500 nm. The polyhedral structure of Cu_7S_4 has a large specific surface area, exposing more active sites so that the occurrence of subsequent tandem catalysis reactions. The size of BSA@Au NPs was about 5 nm and uniformly dispersed as shown in Fig. 1F. Farther, Fig. 1G displayed the prepared BSA@Au NPs were successfully anchored on Cu_7S_4 polyhedron and EDS spectrum in Fig S2C showed Cu, S, Au, O, C and N elements consisting in BSA-Au@Cu_7S_4 polyhedron. In more details, Fig. 1H revealed the even distribution of the Cu, S, Au, O, C and N elements. UV–vis absorption spectra were recorded to assess the optical properties of $SrTiO_3$ NCs, BiOS nanosheet arrays and Cu_7S_4 polyhedron. As shown in Fig S2A, the BiOS nanosheet arrays exhibited the broad light absorption spectrum in comparison to $SrTiO_3$ NCs, which suggested that the existence of BiOS nanosheet arrays on $SrTiO_3$ NCs promoted light absorption in the visible-light region. In Fig S2B, Cu_7S_4 polyhedron had the strong capture in visible-light absorption and the strong absorption peak of BSA-Au@Cu_7S_4 polyhedron at about 540 nm on account of BSA@Au NPs. Therefore, BSA-Au@Cu_7S_4 polyhedron could compete with photoactive matrix for light absorption.

To further explore the chemical state of prepared Cu_7S_4 polyhedron and BSA@Au NPs anchored on the Cu_7S_4 polyhedron successfully, the X-ray photoelectron spectroscopy (XPS) was measured. In Fig. 2A, there were S, Cu and Au peaks in the overall XPS survey pattern, which illustrated the BSA@Au NPs loaded on Cu_7S_4 polyhedron. In detail, the high-resolution XPS spectra of S 2p in Fig. 2B, the peaks at 161.07 eV, 162.55 eV and 164.90 eV were associated with S 2p and the peaks at 167.45 eV belonged to residual SO_4^{2-} specie which its high intensity in Cu_7S_4 advocates the oxidation of surface sulfur [35]. The XPS pattern of Cu 2p was observed in Fig. 2C displayed the peaks at 929.9 eV, 932.11 eV, 950.46 eV and 952.69 eV were attributed to Cu (I) $2p_{3/2}$, Cu (II) $2p_{3/2}$, Cu (I) $2p_{1/2}$ and Cu (II) $2p_{1/2}$ [36]. In addition, the weak peaks at 944.2 eV and 945.7 eV belonged to the satellite band for Cu^{2+} [37,38]. The Au profile clearly displayed in Fig. 4D and the main peaks at 84.90 eV and 87.54 eV were vested in Au $4f_{7/2}$ and Au $4f_{5/2}$ complied with the chemical states of nanosized Au [39], which hinted the BSA-Au@Cu_7S_4

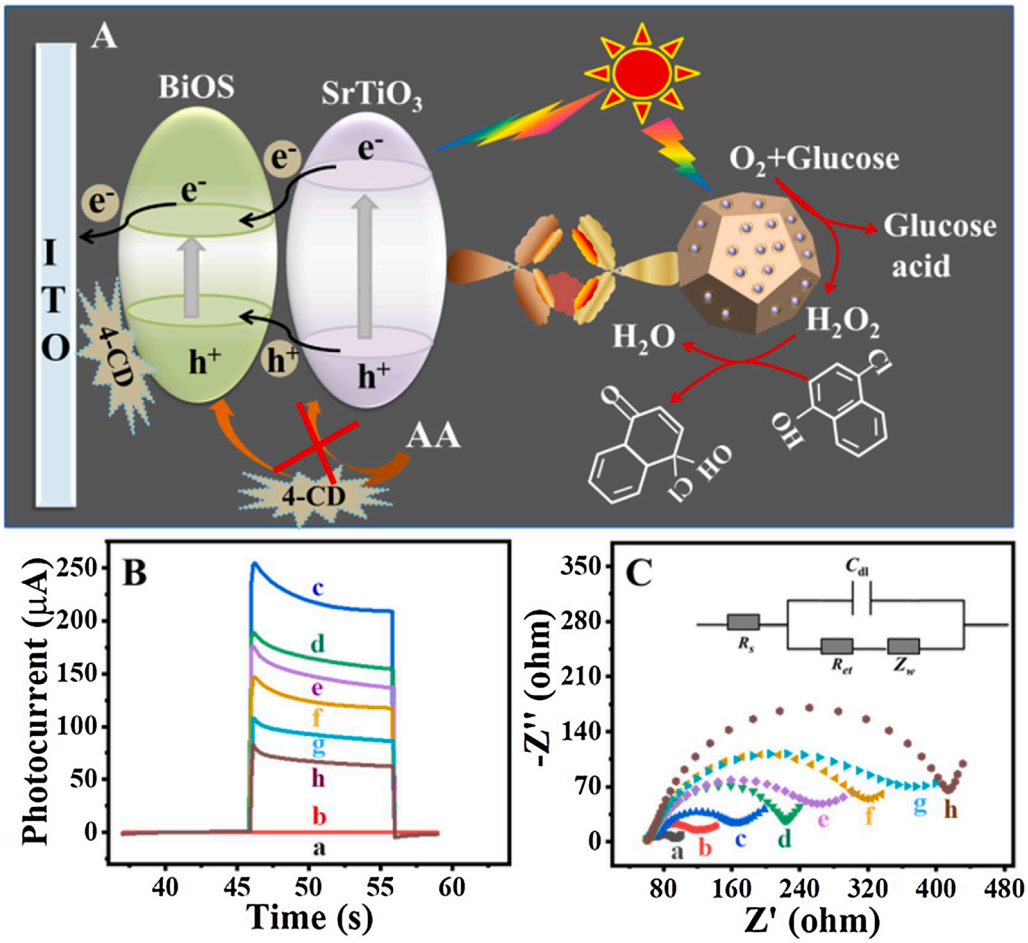

Fig. 3. (A) Possible electron-transfer mechanism of proposed PEC immunosensor; (B) photocurrent responses in the different phases of the electrode modification and (C) EIS characterization: (a) ITO, (b) ITO/$SrTiO_3$, (c) ITO/$SrTiO_3$/BiOS, (d) ITO/$SrTiO_3$/BiOS/Ab_1, (e) ITO/$SrTiO_3$/BiOS/Ab_1/BSA, (f) ITO/$SrTiO_3$/BiOS/Ab_1/BSA/CYFRA21-1, (g) ITO/$SrTiO_3$/BiOS/Ab_1/BSA/CYFRA21-1/BSA-Au@Cu_7S_4-Ab_2 polyhedron, (h) ITO/$SrTiO_3$/BiOS/Ab_1/BSA/CYFRA21-1/BSA-Au@Cu_7S_4-Ab_2 polyhedron immersed in 5 mM glucose and 5 mM 4-CN solution.

polyhedron was fabricated successfully.

3.2. Possible mechanism and characterization of the PEC immunosensor

First of all, the band structures of $SrTiO_3$ NCs and BiOS nanosheets array were measured combining with UV–vis DRS diffuse-reflectance spectra and Mott-Schottky curves. As displayed in Fig S3A and C, the band gap energies of $SrTiO_3$ NCs and BiOS nanosheets array were 3.32 eV and 1.61 eV. The positive slope of line in Fig S3B and D demonstrated the characteristics of their n-type semiconductors [40]. The flat-band potential (V_{fb}) of $SrTiO_3$ NCs and BiOS nanosheets array were -0.89 V and 0.46 V (vs. SCE), respectively. The conduction band potential (E_{CB}) were near to V_{fb} for n-type semiconductors. Therefore, the valence band potential (E_{VB}) of $SrTiO_3$ NCs and BiOS nanosheets array were 2.43 V and 1.15 V (vs. SCE), respectively.

The possible mechanism of electron transfer and the multiple signal inhibition strategy were depicted in Fig. 3A. In the first place, the formation of original PEC signal was explored. To obtain an excellent initial PEC response, BiOS nanosheet arrays was employed to sensitize $SrTiO_3$ NCs as photoactive matrix. Under the irradiation of light, BiOS nanosheet arrays and $SrTiO_3$ NCs gained energy and the electrons of them were excited transitioning from the valence band (VB) to the conduction band (CB) and generating the photoinduced electron-hole (e^-/h^+). Subsequently, the electrons in CB of $SrTiO_3$ NCs injected into CB of BiOS nanosheet arrays and the photoinduced holes in VB of $SrTiO_3$ NCs moved to VB of BiOS nanosheet arrays according to the band structure [41–43]. With the aid of ascorbic acid as an electron donor, the photo-induced holes were swept reducing the photoinduced e^-/h^+ recombination and forming the initial photocurrent. For multiple signal inhibition strategy, BSA-Au@Cu_7S_4 polyhedron as multiple signal regulator controlled the photocurrent response. The photocurrent value about multiple signal inhibition strategy step by step was shown in Fig S4 and the principle and effect of inhibition was elaborated. Firstly, BSA-Au@Cu_7S_4 polyhedron as favorable light absorber possessed a broad absorption range, becoming a competitor with photoactive matrix. Secondly, the precipitation was formed because the BSA-Au@Cu_7S_4 polyhedron possessed duple enzyme-mimicking activities (GOx-like activity and peroxidase-like activity), producing tandem catalysis after incubated with glucose and 4-CN [13]. In detail, the BSA@Au NPs catalyzed glucose to produce H_2O_2 and then catalyzed 4-CN and H_2O_2 to produce 4-CD precipitates on the surface of electrode. And the precipitation hindered electron transfer and light absorption, reducing the PEC response. Thirdly, the steric hindrance effect from BSA-Au@Cu_7S_4 polyhedron also led to the reduction of photocurrent [44].

The change of photocurrent presented by i–t curve was employed to describe the construction process of PEC immunosensor in Fig. 3B. At first, the bare ITO electrode has no photocurrent. After coated by $SrTiO_3$ NCs, the working electrode produced a weak photoelectric response. Followed by the growth of BiOS nanosheet arrays, the photocurrent sharply increased due to the band structure formed between $SrTiO_3$ and BiOS. After incubated with Ab_1, BSA and CYFRA21−1, the photoelectric response was reduced in turn which attributed that biomolecules hinder electron transfer. Finally, since the immobilization of BSA-Au@Cu_7S_4-Ab_2 and the reaction happened in glucose and 4-CN solution, the photoelectric response was decreased by large steric hindrance, competitive absorption with photoactive matrix of BSA-Au@Cu_7S_4 polyhedron and the formation of 4-CD precipitates.

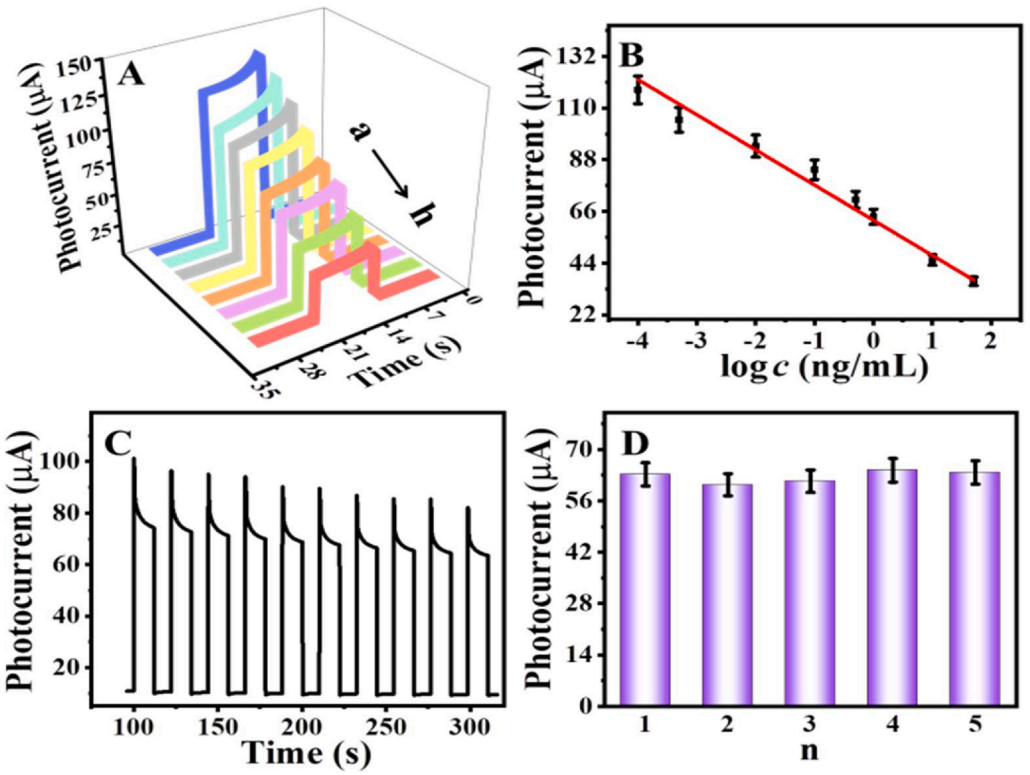

Fig. 4. (A) PEC response curves and (B) Logarithmic calibration curve toward different concentrations of CYFRA21-1 detection: (a) 0.0001, (b) 0.0005, (c) 0.01, (d) 0.1, (e) 0.5, (f) 1, (g) 10, (h) 50 (Units: ng/mL); (C) Stability of PEC immunosensor under illumination cycles on/off 10 times ($c_{CYFRA21-1}$ = 1 ng/mL); (D) Reproducibility analysis.

3.3. Analytical performance of PEC immunosensor

The analytical performance of proposed PEC immunosensor was inspected making use of CYFRA21−1 as a model under the best experimental conditions. Fig. 4A and B revealed the relationship between photocurrent response of the suggested PEC immunosensor and different concentration of CYFRA21−1 from 0.1 pg/mL to 50 ng/mL. Overtly, the photocurrent value was reduced accompanied by the increasing of CYFRA21−1 concentration in Fig. 4A. In the meantime, a linear relationship between the photocurrent and logarithm concentration was established and the fitted linear equation was I = -14.96 log c $_{CYFRA21-1}$ + 62.26 (R^2 = 0.9821) with a low detection limit of 1.12 fg/mL (S/N = 3). Then a comparison with other obtained method for detecting CYFRA21−1 (Table S1), the proposed PEC immunoassay was remarkable to most previous bioanalyses.

3.4. Stability, reproducibility and specificity of PEC immunosensor

Stability is a vital parameter for the propositional PEC immunoassay, which was studied with the method of the continuous on/off cycles of the light for ten times [45,46]. Fig. 4C demonstrated the acceptable results that the photocurrent response did not change significantly. In addition, the storage stability was tested (Figure. S6A) and the photocurrent kept 99.7 %, 97.6 %, 95. 9%, 94.7 % and 92.0 % of its original photocurrent after storing at 4 °C for one day, three days, five days, one weeks and two weeks respectively, thus revealing recognizable storage stability. To investigate the reproducibility of constructed PEC immunosensor, five electrodes including 1.0 ng/mL CYFRA21−1 were manufactured and measured with the identical environment [47]. Fig. 4D showed the measure results (63.22, 64.41, 61.35, 64.34, 63.77 μA) and the RSD was 1.67 % illustrating the satisfactory reproducibility.

Specificity as a necessary performance of the PEC immunosensor was studied [48]. Using amino-terminal pro-B-type natriuretic peptide (NT-pro BNP), cardiac troponin T (cTnT) and amyloid β-protein (Aβ) as interfering substances measured the specificity. The specificity of PEC immunosensor was tested with mixture containing 1 ng/mL CYFRA21−1 and 50-fold interfering substances. Meanwhile, the PEC response was also measured when the electrode was modified with 50 ng/mL interfering substances. The results as exhibited in Fig S6B illustrated the highly selective of the PEC sensing platform.

Table 1
CYFRA21-1 detection in real sample.

Samples (ng/mL)	Added amounts (ng/mL)	Detection amounts (ng/mL)	RSD (%,n = 5)	Recovery (%)
5.86	2	7.78,7.65, 7.99, 7.85, 7.91	1.65	98.80
	5	10.82, 11.03, 10.80, 10.78, 11.14	1.48	101.08
	10	16.18, 15.45, 15.75, 16.01, 15.71	1.79	99.60
2.31	2	4.35,4.29, 4.30, 4.24, 4.38	1.26	100.10
	5	7.09, 7.45, 7.39, 7.53, 7.28	2.32	100.76
	10	11.88, 12.04, 12.63,12.74, 12.38	3.00	100.24

3.5. Real sample analysis

The standard addition method was employed to evaluate the practicality and feasibility of the PEC sensing platform for CYFRA21−1 detection. Briefly, different concentration of CYFRA21−1 was added into human serum sample and then the obtained sample was incubated on suggested PEC sensing platform. As demonstrated in Table 1, the recoveries were found from 98.80% to 101.08% and the RSD were with

the scope of 1.26–3.00 %, which testified the potential of the propositional PEC immunosensor for real sample detection.

4. Conclusion

Conclusively, an ultrasensitive PEC immunosensor was successfully fabricated for CYFRA21−1 detection. The BiOS nanosheet arrays sensitized $SrTiO_3$ ($SrTiO_3$/BiOS) as photoactive material, which improved the absorption of visible light and facilitated the separation and transfer of photogenerated electrons and holes with the aid of electron donor. At the same time, the large specific surface area of $SrTiO_3$/BiOS electrode is beneficial to the immobilization of biomolecules. To improve the detection sensitivity, an innovative tandem biocatalytic precipitation (BCP) strategy by using BSA-Au@Cu_7S_4 polyhedron as the signal regulator to control PEC signals of $SrTiO_3$/BiOS through efficient quenching process. The developed PEC sensing platform displayed sensitive response to CYFRA21−1 concentration. The photocurrent and the logarithm of concentration exhibited a good linear relationship from 0.1 pg/mL to 50 ng/mL with a low detection limit of 1.12 fg/mL. The suggested PEC biosensor provides creative thought to develop an effective method for the early diagnostics of biomarker.

CRediT authorship contribution statement

Yanrong Qian: Conceptualization, Data curation, Writing - original draft. **Yu Du:** Methodology, Writing - review & editing. **Jinhui Feng:** Formal analysis. **Rui Xu:** Formal analysis. **Xiang Ren:** Methodology, Writing - review & editing. **Dawei Fan:** Methodology. **Qin Wei:** Funding acquisition, Project administration. **Huangxian Ju:** Formal analysis.

Declaration of Competing Interest

The authors declare no conflict of interest.

Acknowledgments

We gratefully acknowledge the financial support from the National Key Scientific Instrument and Equipment Development Project of China (No. 21627809), National Natural Science Foundation of China (No. 21777056), Special Foundation for Taishan Scholar Professorship of Shandong Province (No. ts201712052) and Jinan Scientific Research Leader Workshop Project (2018GXRC024).

Appendix A. Supplementary data

Supplementary material related to this article can be found, in the online version, at doi:https://doi.org/10.1016/j.snb.2021.129608.

References

[1] M. Amiri, A. Bezaatpour, H. Jafari, R. Boukherroub, S. Szunerits, Electrochemical methodologies for the detection of pathogens, ACS Sens. 3 (2018) 1069–1086.
[2] Y. Du, J. Xue, X. Sun, D. Wu, X. Liu, H. Ju, et al., Oxygen vacancy-enhanced electrochemiluminescence sensing strategy using luminol thermally encapsulated in Apoferritin as a transducer for biomarker immunoassay, Anal. Chem. 92 (2020) 8472–8479.
[3] R. Xu, Y. Du, D. Leng, L. Liu, Y. Li, X. Ren, et al., Antigen down format photoelectrochemical analysis supported by fullerene functionalized Sn_3O_4, Chem. Commun. (Camb.) 56 (2020) 7455–7458.
[4] D. Hu, H. Liang, X. Wang, F. Luo, B. Qiu, Z. Lin, et al., Highly sensitive and selective photoelectrochemical aptasensor for Cancer biomarker CA125 based on AuNPs/GaN schottky junction, Anal. Chem. 92 (2020) 10114–10120.
[5] J. Shu, Z. Qiu, S. Lv, K. Zhang, D. Tang, Plasmonic enhancement coupling with defect-engineered TiO_{2-x}: a mode for sensitive photoelectrochemical biosensing, Anal. Chem. 90 (2018) 2425–2429.
[6] Y. Jin, D. Jiang, D. Li, P. Xiao, X. Ma, M. Chen, $SrTiO_3$ Nanoparticle/$SnNb_2O_6$ nanosheet 0D/2D heterojunctions with enhanced interfacial charge separation and photocatalytic hydrogen evolution activity, ACS Sustain. Chem. Eng. 5 (2017) 9749–9757.
[7] X.L. Yin, L.L. Li, D.C. Li, D.H. Wei, C.C. Hu, J.M. Dou, Room temperature synthesis of CdS/$SrTiO_3$ nanodots-on-nanocubes for efficient photocatalytic H_2 evolution from water, J. Colloid Interf. Sci. 536 (2019) 694–700.
[8] Z. Zhao, E.J. Willard, H. Li, Z. Wu, R.H.R. Castro, F.E. Osterloh, Aluminum enhances photochemical charge separation in strontium titanate nanocrystal photocatalysts for overall water splitting, J. Mater. Chem. A. 6 (2018) 16170–16176.
[9] J. Han, F. Dai, Y. Liu, R. Zhao, L. Wang, S. Feng, Synthesis of CdSe/$SrTiO_3$ nanocomposites with enhanced photocatalytic hydrogen production activity, Appl. Surf. Sci. 467-468 (2019) 1033–1039.
[10] Y.T. Gong, F. Yuan, Y. Dong, Z. Li, G.L. Wang, Switched photoelectrochemistry of carbon dots for split-type immunoassay, Anal. Chim. Acta 1014 (2018) 19–26.
[11] J.T. Cao, B. Wang, Y.X. Dong, Q. Wang, S.W. Ren, Y.M. Liu, et al., Photogenerated hole-induced chemical redox cycling on Bi_2S_3/$Bi_2Sn_2O_7$ heterojunction: toward general amplified split-type photoelectrochemical immunoassay, ACS Sens. 3 (2018) 1087–1092.
[12] E.A. Bondarenko, E.A. Streltsov, A.V. Mazanik, A.I. Kulak, V. Grivickas, P. Scajev, et al., Bismuth oxysulfide film electrodes with giant incident photon-to-current conversion efficiency: the dynamics of properties with deposition time, Phys. Chem. Chem. Phys. 20 (2018) 20340–20346.
[13] S.-Y. Yu, L. Zhang, L.B. Zhu, Y. Gao, G.C. Fan, D.M. Han, et al., Bismuth-containing semiconductors for photoelectrochemical sensing and biosensing, Coord. Chem. Rev. 393 (2019) 9–20.
[14] L. Zhang, Y.F. Ruan, Y.Y. Liang, W.W. Zhao, X.D. Yu, J.J. Xu, et al., Bismuth oxyiodide couples with glucose oxidase: a special synergized dual-catalysis mechanism for photoelectrochemical enzymatic bioanalysis, ACS Appl. Mater. Inter. 10 (2018) 3372–3379.
[15] X. Zhang, X. Wang, D. Wang, J. Ye, Conformal $BiVO_4$-Layer/WO_3-Nanoplate-Array heterojunction photoanode modified with cobalt phosphate cocatalyst for significantly enhanced photoelectrochemical performances, ACS Appl Mater Inter 11 (2019) 5623–5631.
[16] W.W. Zhao, J.J. Xu, H.Y. Chen, Photoelectrochemical immunoassays, Anal. Chem. 90 (2018) 615–627.
[17] L.A, F. Patolsky, I. Willner, Highly sensitive amplified electronic detection of DNA by biocatalyzed precipitation of an insoluble product onto electrodes, Chem. Eur. J. 9 (2003) 1137–1145.
[18] W.W. Zhao, Z.Y. Ma, P.P. Yu, X.Y. Dong, J.J. Xu, H.Y. Chen, Highly sensitive photoelectrochemical immunoassay with enhanced amplification using horseradish peroxidase induced biocatalytic precipitation on a CdS quantum dots multilayer electrode, Anal. Chem. 84 (2012) 917–923.
[19] N. Zhang, Y.F. Ruan, Z.Y. Ma, W.W. Zhao, J.J. Xu, H.Y. Chen, Simultaneous photoelectrochemical and visualized immunoassay of beta-human chorionic gonadotrophin, Biosens. Bioelectron. 85 (2016) 294–299.
[20] R. Lu, D. Yang, D. Cui, Z. Wang, L. Guo, Egg white-mediated green synthesis of silver nanoparticles with excellent biocompatibility and enhanced radiation effects on cancer cells, Int. J. Nanomed. 7 (2012) 2101–2107.
[21] W. Peng, Y. Qin, W. Li, M. Chen, D. Zhou, H. Li, et al., Nonenzyme cascaded amplification biosensor based on effective aggregation luminescence caused by disintegration of silver nanoparticles, ACS Sens. 5 (2020) 1912–1920.
[22] R. Viswambari Devi, M. Doble, R.S. Verma, Nanomaterials for early detection of cancer biomarker with special emphasis on gold nanoparticles in immunoassays/sensors, Biosens. Bioelectron. 68 (2015) 688–698.
[23] Y. Zhao, Y. Huang, H. Zhu, Q. Zhu, Y. Xia, Three-in-one: sensing, self-assembly, and cascade catalysis of cyclodextrin modified gold nanoparticles, J. Am. Chem. Soc. 138 (2016) 16645–16654.
[24] H. Zhang, X. Liang, L. Han, F. Li, "Non-Naked" gold with glucose oxidase-like activity: a nanozyme for tandem catalysis, Small 14 (2018) e1803256.
[25] Y. Jiang, S. Zhang, Q. Ji, J. Zhang, Z. Zhang, Z. Wang, Ultrathin Cu_7S_4 nanosheets-constructed hierarchical hollow cubic cages: one-step synthesis based on Kirkendall effect and catalysis property, J. Mater. Chem. A. 2 (2014) 4574–4579.
[26] Y. Li, W. Zhu, Q. Kang, L. Yang, Y. Zhang, Y. Wang, et al., Dual-mode electrochemical immunoassay for insulin based on Cu_7S_4-Au as a double signal Indicator, ACS Appl Mater Inter 10 (2018) 38791–38798.
[27] X. Yu, J. Bi, G. Yang, H. Tao, S. Yang, Synergistic effect induced high photothermal performance of Au Nanorod@Cu_7S_4 yolk–Shell nanooctahedron particles, J. Phys. Chem. C. 120 (2016) 24533–24541.
[28] W. Song, B. Zhao, C. Wang, Y. Ozaki, X. Lu, Functional nanomaterials with unique enzyme-like characteristics for sensing applications, J. Mater. Chem. B. 7 (2019) 850–875.
[29] X. Li, Z. Yao, J. Wang, D. Li, K. Yu, Z. Jiang, A novel flake-like Cu_7S_4 solar absorber for high-performance large-scale water evaporation, ACS Appl. Energy Mater. 2 (2019) 5154–5161.
[30] G. Liu, J. Xu, K. Wang, Solar water evaporation by black photothermal sheets, Nano Energy 41 (2017) 269–284.
[31] Y. Hao, X. Wang, L. Li, Highly dispersed $SrTiO_3$ nanocubes from a rapid sol-precipitation method, Nanoscale 6 (2014) 7940–7946.
[32] E.A. Bondarenko, E.A. Streltsov, M.V. Malashchonak, A.V. Mazanik, A.I. Kulak, E. V. Skorb, Giant Incident Photon-to-Current Conversion with Photoconductivity Gain on Nanostructured Bismuth Oxysulfide Photoelectrodes under Visible-Light Illumination, Adv. Mater. 29 (2017), 1702387.
[33] C. Shi, X. Zhou, W. Li, H. Guo, Y. Zhao, L. Ruan, et al., Synergistic enhancing photoelectrochemical response of $Bi_{10}O_6S_9$ with WO_3 optical heterojunction in wide wavelength range, Appl. Surf. Sci. 509 (2020).
[34] Y. Qian, J. Feng, H. Wang, D. Fan, N. Jiang, Q. Wei, et al., Sandwich-type signal-off photoelectrochemical immunosensor based on dual suppression effect of PbS

quantum dots/Co_3O_4 polyhedron as signal amplification for procalcitonin detection, Sens. Actuat B Chem. 300 (2019), 127001.
[35] L.L. Feng, G. Yu, Y. Wu, G.D. Li, H. Li, Y. Sun, et al., High-index faceted Ni_3S_2 nanosheet arrays as highly active and ultrastable electrocatalysts for water splitting, J. Am. Chem. Soc. 137 (2015) 14023–14026.
[36] Q. Li, X. Wang, K. Tang, M. Wang, C. Wang, C. Yan, Electronic modulation of electrocatalytically active center of Cu_7S_4 nanodisks by cobalt-doping for highly efficient oxygen evolution reaction, ACS Nano 11 (2017) 12230–12239.
[37] J. Xu, J. Cui, C. Guo, Z. Zhao, R. Jiang, S. Xu, et al., Ultrasmall Cu_7S_4 @MoS_2Hetero-Nanoframes with Abundant Active Edge Sites for Ultrahigh-Performance Hydrogen Evolution, Angew. Chem. Int. Ed. Engl. 55 (2016) 6502–6505.
[38] D. Kelly, A. Singh, C.A. Barrett, C. O'Sullivan, C. Coughlan, F.R. Laffir, et al., A facile spin-cast route for cation exchange of multilayer perpendicularly-aligned nanorod assemblies, Nanoscale 3 (2011) 4580–4583.
[39] Y.-H. Chiu, Y.-J. Hsu, Au@Cu_7S_4 yolk@shell nanocrystal-decorated TiO_2 nanowires as an all-day-active photocatalyst for environmental purification, Nano Energy 31 (2017) 286–295.
[40] T. Wu, Y. Zhang, D. Wei, X. Wang, T. Yan, B. Du, et al., Label-free photoelectrochemical immunosensor for carcinoembryonic antigen detection based on g-C_3N_4 nanosheets hybridized with $Zn_{0.1}Cd_{0.9}S$ nanocrystals, Sens. Actuat B: Chem. 256 (2018) 812–819.
[41] Y. Hou, A.B. Laursen, J. Zhang, G. Zhang, Y. Zhu, X. Wang, et al., Layered nanojunctions for hydrogen-evolution catalysis, Angew. Chem. Int. Ed. Engl. 52 (2013) 3621–3625.
[42] H. Naderi, S. Hajati, M. Ghaedi, J.P. Espinos, Highly selective few-ppm NO gas-sensing based on necklace-like nanofibers of ZnO/CdO n-n type I heterojunction, Sens. Actuat B: Chem. 297 (2019), 126774.
[43] Y. Zhu, T. Wan, X. Wen, D. Chu, Y. Jiang, Tunable Type I and II heterojunction of CoOx nanoparticles confined in g-C_3N_4 nanotubes for photocatalytic hydrogen production, Appl. Catal. B: Environ. 244 (2019) 814–822.
[44] R. Yang, K. Zou, Y. Li, L. Meng, X. Zhang, J. Chen, Co_3O_4-Au Polyhedra: A Multifunctional Signal Amplifier for Sensitive Photoelectrochemical Assay, Anal. Chem. 90 (2018) 9480–9486.
[45] L. Guo, H. Yin, M. Xu, Z. Zheng, X. Fang, R. Chong, et al., In situ generated plasmonic silver nanoparticle-sensitized amorphous titanium dioxide for ultrasensitive photoelectrochemical sensing of formaldehyde, ACS Sens. 4 (2019) 2724–2729.
[46] Y. Qian, J. Feng, R. Xu, D. Fan, Y. Du, X. Ren, et al., Zinc and molybdenum Co-doped $BiVO_4$ nanoarray for photoelectrochemical diethylstilbestrol analysis based on the dual-competitive system of manganese hexacyanoferrate hydrate nanocubes, ACS Appl. Mater. Inter. 12 (2020) 16662–16669.
[47] M. Jalali, R.S. Moakhar, T. Abdelfattah, E. Filine, S.S. Mahshid, S. Mahshid, Nanopattern-assisted direct growth of peony-like 3D MoS_2/Au composite for nonenzymatic photoelectrochemical sensing, ACS Appl. Mater. Inter. 12 (2020) 7411–7422.
[48] Y. Yuan, T. Hu, X. Zhong, M. Zhu, Y. Chai, R. Yuan, Highly sensitive photoelectrochemical biosensor based on quantum dots sensitizing Bi_2Te_3 nanosheets and DNA-Amplifying strategies, ACS Appl. Mater. Inter. 12 (2020) 22624–22629.

Yanrong Qian studies in school of chemistry and chemical engineering, University of Jinan as postgraduate student.

Yu Du works and studies in School of Chemistry and Chemical Engineering, University of Jinan as a teacher. Her main research interests are the determination of chemical immunosensor.

Jinhui Feng studies in school of chemistry and chemical engineering, University of Jinan as doctoral student.

Rui Xu is a doctoral candidate in school of chemistry and chemical engineering, University of Jinan. Her current researchers are photoelectrochemical sensor and nanomaterials.

Xiang Ren received his B.S. degrees in Chemistry of Materials/English from University of Jinan in 2012, M.S. degree in Chemical Engineering and Technology from University of Jinan in 2015, and Ph.D. degree from University of Jinan/University of Electronic Science and Technology of China in 2019. Now, he is an associate professor in University of Jinan. His main research interests are energy catalysis, nanomaterials controlled-synthesis, and electrochemical biosensors.

Dawei Fan received Ph.D. degree from Lanzhou Institute of Chemical Physics, Chinese Academy of Sciences in 2010. Now, she is an associate professor at University of Jinan. Her main research interests are the determination of photoelectrochemical immunosensor.

Qin Wei, a professor and DSc, has devoted herself to analytical teaching and scientific research. Her main research interests are the determination of protein and nucleic acid by photometry and the electrochemical immunosensor preparation. She has published over two hundred articles on analysis, immunosensor and applied successfully for many research projects, such as *Biomaterials, Advanced Functional Materials., Biosensors & Bioelectronics, Sensors and Actuators B-Chemical ACS Applied Materials & Interfaces, and Talanta*.

Huangxian Ju received his BS, MS and PhD degrees from Nanjing University during 1982–1992. He was a postdoc in Montreal University (Canada) in 1996–1997 and a guest professor in three universities of Germany and Ireland in 1999–2000. He became an associate and full professor of Nanjing University in 1993 and 1999. He is currently the director of State Key Laboratory of Analytical Chemistry for Life Science. His research interests focus on analytical biochemistry, biosensing and molecular diagnosis. He has published 635 papers in different journals with h-index of 85 (Google Scholar h-index 95 with about 31,634 citations).